

Calculation of the Local Standard of Rest from 20,574 Local Stars in the New Hipparcos Reduction with Known Radial Velocities

Charles Francis¹, Erik Anderson²

¹ 25 Elphinstone Rd., Hastings, TN34 2EG, UK.

² 6372 Quail Creek Drive, Redding, CA 96002, USA.

21 December 2008

ABSTRACT

Context. An accurate estimate of the local standard of rest (LSR) is required to determine key parameters used to approximate Galactic mass models and to understand Galactic structure and evolution. However, authors are often forced to base dynamical analyses on potentially unreliable figures because recent determinations of the LSR have failed to reach agreement, especially with regard to the direction, V , of Galactic rotation.

Aims. This paper aim is to explain why the traditional method for calculating the LSR fails, and to find alternative means of calculating the LSR with realistic error margins. To this end, we assemble and investigate the kinematic properties of 20,574 stars within 300pc, with complete and accurate kinematic data.

Methods. The traditional method of calculating the LSR assumes a well-mixed distribution. In fact, the velocity distribution is highly structured, invalidating calculations based on mean motions and asymmetric drift. We find other indicators in the distribution which we believe give a better estimate of circular motion.

Results. We find good agreement between results and give as our best estimate of the LSR $(U_0, V_0, W_0) = (7.5 \pm 1.0, 13.5 \pm 0.3, 6.8 \pm 0.1) \text{ km s}^{-1}$. We calculate the slope of the circular speed curve, finding $-9.3 \pm 0.9 \text{ km s}^{-1} \text{ kpc}^{-1}$.

Key Words: Astrometry – celestial mechanics – stars: kinematics – stars: statistics – Galaxy: kinematics and dynamics – Galaxy: solar neighbourhood.

1 Introduction

The local standard of rest (LSR) is defined to mean the velocity of a circular orbit at the Solar radius from the Galactic centre. The definition idealizes an axisymmetric galaxy in equilibrium, ignoring features like the bar, spiral arms, and perturbations due to satellites. An accurate estimate of the LSR is required to determine parameters like the enclosed mass at the solar radius for use in approximate mass models (e.g., Klypin, Zhao & Somerville, 2002) and the eccentricity distribution which is of importance in understanding Galactic structure and evolution. In the absence of a rigorous determination of the LSR, authors are often forced to base dynamical analyses on a potentially unreliable figure. Recent determinations of the LSR have failed to reach agreement, especially with regard to the direction, V , of Galactic rotation. Quoted error margins in table 1 are much less than the variation in the figures found for the LSR. A number of factors may contribute to this, including lack of complete kinematic information, selection criteria, and the irregular velocity distribution of the population due to bulk motions – either moving groups formed from particular gas clouds or streams arising from large scale dynamics (Dehnen 1998, Famaey et al., 2005).

The usual way to calculate the LSR is to calculate the mean velocity of a stellar population, and to correct for asymmetric drift. This method requires a well-mixed distribution and is vulnerable to kinematic bias due to bulk motions within star populations. Usually it is hoped that in an average, over many streams each representing

only a minor fraction of the whole sample, the effect of bulk motions will largely average out. This assumption is not borne out in the data. After removal of fast moving stars, a few streams contribute over one third of the entire population (Famaey et al., 2005), and inevitably bias a traditional analysis. Moreover, the composition of the streams is strongly dependent on both age and colour (Dehnen 1998). We will show that this seriously affects calculations of the asymmetric drift from the velocity and dispersion of different populations. We will conclude that the principal reason for disagreement between the analyses tabulated in table 1 is that the influence of streams has not been understood.

To rectify this deficiency and to check the accuracy of results, we have considered a number of indicators using a large population of single stars and solved spectroscopic binaries with complete kinematic data. The methods are summarized in section 3. We find good agreement between indicators.

2 The Stellar Population

To minimize the influence of random errors on the results it is important to use stars for which accurate measurement is available. Hipparcos provided parallax measurements of unsurpassed accuracy. Systematic parallax errors are stated at less than 0.1 mas (ESA, 1997), or less than 3% for a star at 300pc. We restricted the populations to stars for which standard parallax errors were less than 20% of the quoted parallax. A distance cut of 300pc was also applied.

Source	Notes	Data	U_0	V_0	W_0
Bobylev & Bajkova (2007)	F & G dwarfs,	3D motions	8.7 ± 0.5	6.2 ± 2.2	7.2 ± 0.8
Bobylev, et al. (2006)	from the PCRV,	3D motions	10.2 ± 0.4	10.9 ± 0.4	6.6 ± 0.4
Hogg, et al. (2005)		proper motions	10.1 ± 0.5	4.0 ± 0.8	6.7 ± 0.2
Fehrenbach, et al. (2001)	Avg. Dist. = 46 pc,	radial velocities	9.79 ± 0.5	13.20 ± 0.5	3.25 ± 0.9
Fehrenbach, et al. (2001)	Avg. Dist. = 195 pc	radial velocities	8.24 ± 0.6	11.58 ± 0.6	5.97 ± 1.1
Fehrenbach, et al. (2001)	Avg. Dist. = 378 pc	radial velocities	2.93 ± 0.6	10.36 ± 0.6	4.79 ± 1.2
Mignard (1999)	A0-F5, 100pc - 2kpc,	proper motions	11.0	10.87	7.23
Mignard (1999)	K0-K5	proper motions	9.88	14.19	7.76
Miyamoto and Zhu (1998)	159 Hipparcos Cepheids	proper motions	10.62 ± 0.49	16.06 ± 1.14	8.60 ± 1.02
Dehnen & Binney (1998)	Max Dist. ~ 100pc, Hipparcos	proper motions	10.00 ± 0.36	5.23 ± 0.62	7.17 ± 0.38
Binney et al. (1997)	Stars near south celestial pole	proper motions	11 ± 0.6	5.3 ± 1.7	7.0 ± 0.6
Jaschek, et al. (1991a)	Mean, Bright Star Catalogue	radial velocities	11.4	14.7	7.6
Jaschek, et al. (1991b)	Median	radial velocities	9.8	11.6	5.9
Jaschek, et al. (1991b)	Mode	radial velocities	8.6	7.2	3.8
Mihalas & Binney (1981)	Galactic astronomy: 2nd ed.		9.2 ± 0.3	12.0	6.9 ± 0.2
Mayor (1974)	A & F stars	3D motions	10.3 ± 1	6.3 ± 0.9	5.9 ± 0.4

Table 1: Recent measurements of the LSR fail to converge, particularly in the V -direction.

After the distance cuts, the populations contained very few stars with large motion errors.

We derived a stellar population with kinematically complete data by combining astrometric parameters from the recently released catalogue, *Hipparcos, the New Reduction of the Raw Data* (van Leeuwen, 2007a; hereafter “HNR”) plus the Tycho-2 catalogue (ESA, 1997) with radial velocity measurements contained in the *Second Catalogue of Radial Velocities with Astrometric Data* (Kharchenko, et al., 2007; hereafter “CRVAD-2”).

HNR claims improved accuracy by a factor of up to 4 over the original Hipparcos catalogue (ESA, 1997) for nearly all stars brighter than magnitude 8. The improvement is primarily due to the increase of available computer power since the original calculations from the raw data. *Validation of the new Hipparcos reduction* (van Leeuwen, 2007b) “confirms an improvement by a factor 2.2 in the total weight compared to the catalogue published in 1997, and provides much improved data for a wide range of studies on stellar luminosities and local galactic kinematics.” Our analysis showed evidence of the improvement in the data by comparison with a preliminary analysis based on the previous dataset, both by substantially increasing the number of stars with parallax errors less than 20%, and by showing moving groups as sharper spikes in the velocity distribution – errors will tend to smear out such spikes.

CRVAD-2 contains most of the stars in two important radial velocity surveys: *The Geneva-Copenhagen survey of the Solar neighbourhood* (Nordström, et al., 2004; hereafter G-CS), which

surveyed nearby F and G dwarfs, and *Local Kinematics of K and M Giants from CORAVEL* (Famaey et al., 2005; hereafter: “Famaey”). We included about 300 stars in G-CS and Famaey not given in CRVAD-2 and incorporated the revised ages for G-CS II (Holmberg, Nordström and Andersen, 2007).

G-CS and Famaey are deemed to be free from kinematic selection bias. The remaining radial velocities in CRVAD-2 are derived from the *General Catalog of Mean Radial Velocities* (Barbier-Brossat and Fignon, 2000; hereafter “GCRV”) and the *Pulkovo Catalog of Radial Velocities* (Bobylev, et al. 2006). These are compilations from sources which may contain a selection bias favoring high proper-motion stars (Binney et al., 1997). Our best methods for determining the LSR exclude high velocity stars. Concern over a bias towards high proper motions is overstated, since the traditional calculation is fairly insensitive to a kinetic bias with no directional component; a bias toward high velocity stars will increase uncertainty, but the consequent high figures for both \bar{V} and for the asymmetric drift will tend to cancel out in the calculation of V_0 . It is seen in the analysis that any bias to high motion stars in CRVAD-2 has no impact on results. Binney et al. did not give a statistical analysis for their conclusion, but justified it from a graph (their fig. 2) with a logarithmic scale which exaggerates evidence of bias by two orders of magnitude. Comparison of the statistics for the entire population and for G-CS and Famaey shows little, if any, evidence of selection bias toward high proper motion, (table 2 and table 3), and none when high velocity stars are excluded. Any bias appears to be

Population	Stars	proportion	$ pm $	$\sigma_{ pm }$	$ v_t $	$\sigma_{ v_t }$
All F&G dwarfs	9663	100%	120.4	136.6	36.1	30.9
G-CS F&G dwarfs	8148	100%	123.8	138.7	34.8	27.3
All K&M giants	4916	100%	61.6	61.6	35.6	25.4
Famaey K&M giants	1534	100%	55.1	65.1	35.3	24.7
All F&G dwarfs	7296	75.5%	104.6	101.8	26.2	14.2
G-CS F&G dwarfs	6190	75.9%	109.3	104.5	26.6	14.3
All K&M giants	3489	70.1%	39.3	36.4	26.0	14.3
Famaey K&M giants	1098	70.6%	45.7	38.4	25.8	14.7

Table 2: Top table: Comparison of means and standard deviations of the magnitude of transverse velocity, v_t , and magnitude of proper motion, pm , for all F&G dwarfs and G-CS, and for all K&M giants and Famaey. Bottom table: Comparison when the population is restricted to the velocity ellipsoid (section 4). Evidence of selection bias is outweighed by uncertainties due to fast moving stars.

toward high transverse velocities, not high proper motions. The most likely cause is statistical errors due to the high proportion of fast moving stars in the population. Skuljan, Hearnshaw and Cottrell (1999) have also analysed the claim, finding that “the effect is important only at $v_t > 70\text{-}80\text{ km s}^{-1}$ ”.

A more important consideration is kinetic bias with a directional component. A number of kinematic studies have concentrated on stars in open clusters. These are likely to be over-represented in CRVAD-2. Even without selection bias, the existence of clusters and streams adds kinematic bias. To determine the LSR we must find an indicator which is not affected by streams.

Our population of 20,574 stars is obtained by applying the following selection criteria:

(i) Heliocentric distance within 300 pc based on NRH parallaxes and parallax error less than 20% of parallax. (details below).

(ii) Radial velocity given in CRVAD-2, GC-S or Famaey and uniquely identified to a Hipparcos catalogue number. CRVAD-2 figures were used by default, as CRVAD-2 gives a weighted mean for stars in Famaey having radial velocities from other sources. We excluded stars for which no radial velocity error was given, or for which the quoted error was greater than 5 km s^{-1} .

(iii) The object is either a single star or a spectroscopic binary with a computed mean radial velocity. This criterion is determined from flags provided by G-CS, Famaey, Tycho-2, and CRVAD-2.

(iv) It is usual in statistical analyses of data to eliminate outliers more than three (or fewer) standard deviations from the mean, because outliers tend to have a disproportionately large affect on results. This cannot be done here because the distributions are far from Gaussian and contain a high proportion of fast moving stars. Velocities opposing any error in the mean will be preferentially removed, resulting in a compounded error and leading to non-convergence on iteration of the method. It remains important to remove stars with extreme velocities, especially those with contrary orbits or with orbits excessively inclined to the galactic plane. A more disperse distribution was found for stars aged over 10Gyrs. We applied a cut on stars with velocities outside of an ellipsoid

$$\frac{(U + 12)^2}{200^2} + \frac{(V + 42)^2}{200^2} + \frac{(W + 7)^2}{120^2} < 1, \quad (2.1)$$

corresponding approximately to a 4 s.d. cut on each axis for the population of old stars, and to over 6 s.d. for the remaining population. This removed 86 stars.

Because parallax distance is measured as an inverse law of parallax angle, errors are not symmetrical and a systematic distance error is introduced (this is a part, but not the main part, of the Lutz-Kelker bias which concerns estimates of absolute magnitude). For example, for two measurements with 20% error above and below the true parallax, one finds a mean error of 4%:

$$R = \left(\frac{1000}{Plx(1-0.2)} + \frac{1000}{Plx(1+0.2)} \right) \div 2 = \frac{1000}{Plx(1-0.2^2)}. \quad (2.2)$$

For a Gaussian error distribution with $\sigma = 20\%$ we calculate a expected systematic error of 1.6%. This represents an upper bound on the systematic error. Over 70% of the stars in the population have parallax errors less than 10%. The systematic error goes as the square of the random error and can be estimated at below 1%. We compensated using a pragmatic approximation,

$$R = \frac{1000}{Plx(1 - 0.4(ePlx/Plx)^2)}. \quad (2.3)$$

The accuracy of Hipparcos and Tycho proper motions is generally little better than that of ground-based astrometry on account of the short duration (3.3 yr) of the Hipparcos mission. We used a mean value from HNR and Tycho for proper motion, inversely

weighted by the squared quoted error, to obtain the best possible figure. The mean error in transverse velocity is 0.34 km s^{-1} , about 1% of the mean transverse velocity, 32.9 km s^{-1} . The mean error in radial velocity for the population is 1.3 km s^{-1} , for stars also in G-CS the error is 0.87 km s^{-1} and and for stars also in Famaey it is 0.26 km s^{-1} .

We established subpopulations of 8,098 dwarfs and 6,572 giants and subgiants from five databases of stellar types: *NStars Project* (Gray, et al., 2003 & 2006), *Michigan Catalogue of HD stars*, Vols. 1-5 (Houk & Cowley, 1975; Houk, 1978, 1982, 1988, 1999), *Catalogue of Stellar Spectral Classifications* (Skiff, 2007), *Selected MK Spectral Types* (Jaschek, 1975), and *The Tycho-2 Spectral Type Catalog* (Wright, 2003) by preference in that order.

3 Methodologies

In a traditional determination of the LSR, the mean velocities of a kinematically unbiased stellar sample are calculated assuming a well-mixed distribution and a correction is made for asymmetric drift (e.g., Binney & Tremaine, 1987, pp. 198-9). In equilibrium, the distribution should vary smoothly between maximum at apocentre and minimum at pericentre, because stellar density increases as orbital radius decreases and because stars move more slowly at apocentre. This distribution is not observed (figures 11, 12, 21, 22). Even if star selection is kinematically unbiased, bulk motions appear prominently in the velocity distributions at all colours, and bias the calculation of both mean velocity and the asymmetric drift. Methods I & II show the the effect of bias on the traditional calculation. Methods III, IV, V and VI consider alternative indicators.

I. Traditional Calculation (section 6): We calculated the LSR using Strömberg’s asymmetric drift equation (6.1), using the theoretical value of D given by Binney and Tremaine, for the whole population and for the population inside the velocity ellipsoid (section 4), for which we found a reduced error margin. We calculated the asymmetric drift by binning the population by colour and by type, and finding the best fit linear regression, following Dehnen & Binney (1998). The resulting figures for the LSR do not appear reasonable, since they indicate a disproportionately large number of stars on the outer part of their orbit.

II. Old stars (section 8): The population of old stars shows different kinematic properties from the whole sample. Streaming motions are not eliminated and it is not possible to form an estimate of the LSR. It is found that the origin of Parenago’s discontinuity is the existence of fast moving streams of older stars, not continuous heating of the disc.

III. Young stars (section 7): Young stars are formed from gas clouds which are expected to be in more nearly circular motion than stellar populations. We find that the velocity dispersion of hot stars is much less than that of the population as a whole. While this does not give a precise estimate of the LSR, it is an indicator of the region of velocity space in which we might expect to find the LSR.

IV. Eccentricity cut (section 10): Although prone to similar problems due to streaming as the velocity distribution, the eccentricity distribution is considerably more even. The assumption that streaming motions will largely cancel is less doubtful and there is better reason to think that an eccentricity cut will give a homogeneous population of thin disc stars. The method has fewer degrees of freedom, and no auxiliary assumptions are needed to compensate for the asymmetric drift.

V. Circular orbits (section 11): Disc heating is the process by which scattering events cause the random velocities of stars to increase with age (e.g., Jenkins, 1992). Even in thermal equilib-

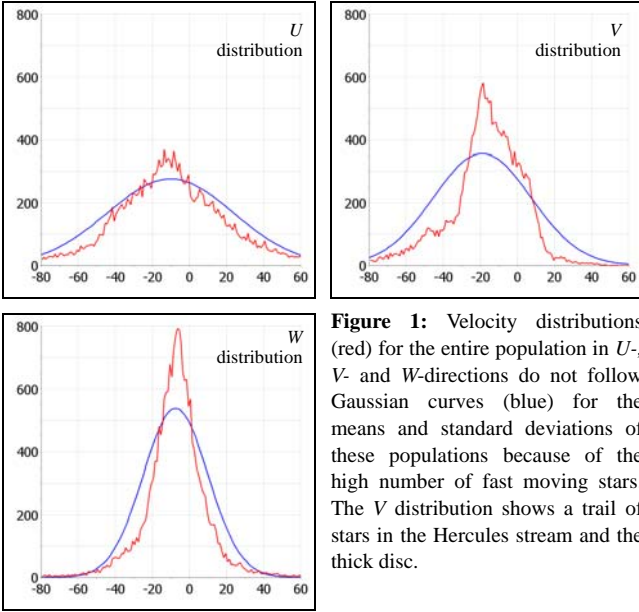


Figure 1: Velocity distributions (red) for the entire population in U -, V - and W -directions do not follow Gaussian curves (blue) for the means and standard deviations of these populations because of the high number of fast moving stars. The V distribution shows a trail of stars in the Hercules stream and the thick disc.

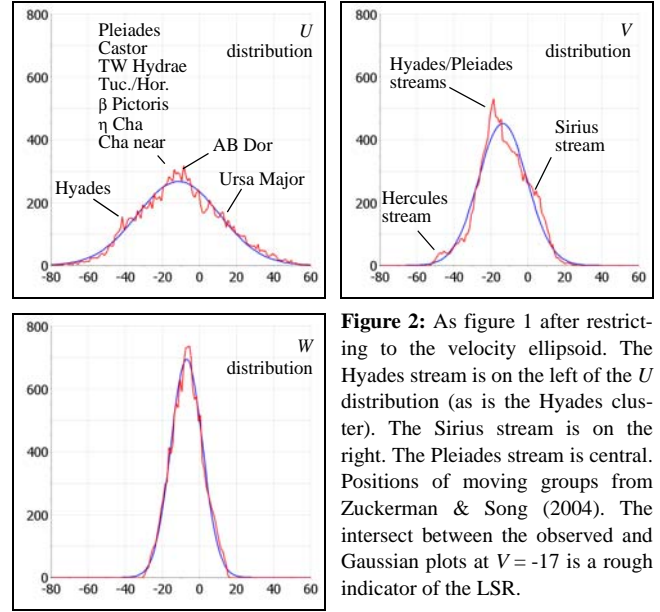


Figure 2: As figure 1 after restricting to the velocity ellipsoid. The Hyades stream is on the left of the U distribution (as is the Hyades cluster). The Sirius stream is on the right. The Pleiades stream is central. Positions of moving groups from Zuckerman & Song (2004). The intersect between the observed and Gaussian plots at $V = -17$ is a rough indicator of the LSR.

rium, one would expect a modal value of random peculiar velocity denoting disc temperature. As a result, the distribution in velocity space can be expected to have a minimum at circular motion. In fact a number of minima are observed. These minima do not directly yield a precise estimate of the LSR. We calculated the distribution of the number of stars with eccentricity less than 0.01 for different values of the LSR and found the most significant well at a precise value which we believe to be the best available estimate of the LSR. The depth of the well increases when early type stars are excluded, as would be expected if stars are typically formed in gas clouds with near to circular motion. This estimate is independent of kinetic bias due to streams or selection, and gives our best estimate of the LSR.

VI. Circular speed curve (section 12): For a range of values of U close to orbital extrema, corresponding to the observed minimum at the LSR, there is a clear trough in the distribution of transverse components of orbital velocities plotted against distance to SgrA*. U_0 is chosen to optimise the trough. V_0 and the local slope of the circular speed curve are found by regression on the minima. With results from Gaia, this method can potentially be extended to give the circular rotation curve of the Milky Way.

4 The Schwarzschild Velocity Ellipsoid

For the population of 20,574 stars, the mean velocity is $(\bar{U}, \bar{V}, \bar{W}) = (-10.2 \pm 0.2, -18.3 \pm 0.2, -7.4 \pm 0.1)$ km s⁻¹. Standard deviation is $(U_{s.d.}, V_{s.d.}, W_{s.d.}) = (32.6, 22.4, 16.5)$. Calculation of errors is hampered because the velocity distributions are far from Gaussian and contain bulk motions as well as substantial numbers (27.5%) of fast moving stars, including halo stars, thick disc stars, stars produced in high energy events and stars with unusual orbits following collisions or near collisions. As a result, the calculated statistical error understates the true error.

We restricted the populations to mainly thin disc stars with conventional motions in a velocity ellipsoid by fitting the truncated distributions to Gaussian curves. Gaussian fitting is more laborious, but has a number of advantages over truncating to with three standard deviations of the mean. The method converges to a definite central point for the velocity ellipsoid, while fitting to a mean does not. It is less influenced by moving groups and results in close to Gaussian distributions within an approximately 3σ ellipsoid, particularly for the U and W distributions. The error in the mean due to the error in the fitted ellipsoid is less than the statistical error in the mean. Velocity distributions were found using 1 km s⁻¹ bins (figure 1) and fitted by minimizing the sum of squared differences per degree of freedom between the observed distributions of U -, V - and

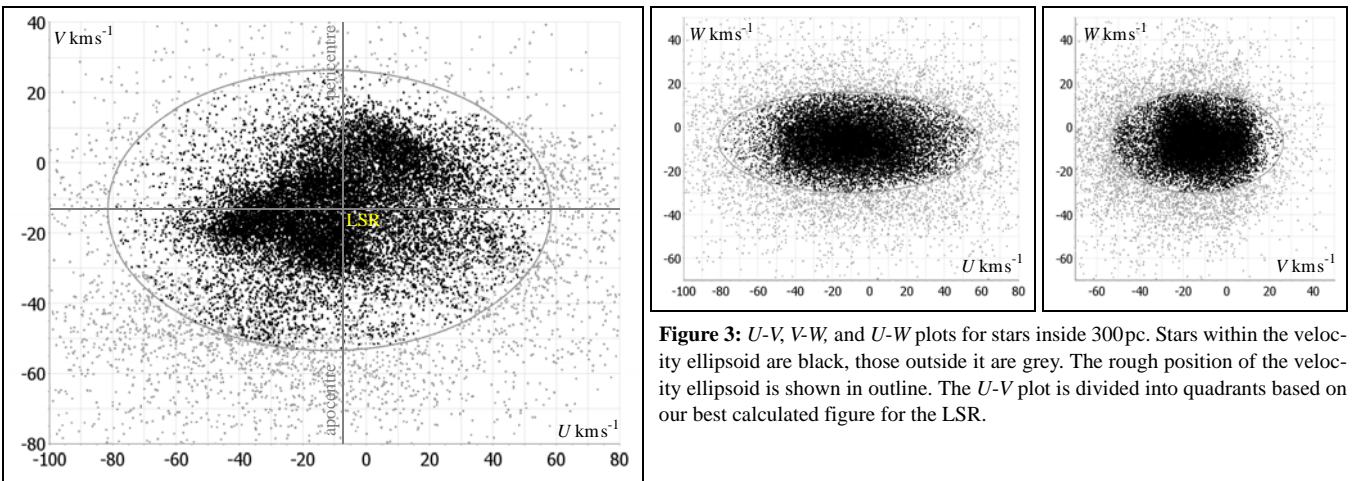


Figure 3: U - V , V - W , and U - W plots for stars inside 300pc. Stars within the velocity ellipsoid are black, those outside it are grey. The rough position of the velocity ellipsoid is shown in outline. The U - V plot is divided into quadrants based on our best calculated figure for the LSR.

W -velocities within the velocity ellipsoid and Gaussian distributions with the same central point and with the same standard deviations (figure 2). Six variables were used for the fit, defining the centre of the ellipsoid and the length of three axes. Confidence limits were found from a χ^2 probability distribution, after normalising squared differences. The centre of the fitted ellipsoid is $(U_e, V_e, W_e) = (-11.2 \pm 0.4, -13.6 \pm 0.3, -6.9 \pm 0.1) \text{ km s}^{-1}$. The semi-axes are $(70, 40, 23) \text{ km s}^{-1}$.

After restricting the population to

$$\frac{(U + 11.2)^2}{70^2} + \frac{(V + 13.6)^2}{40^2} + \frac{(W + 6.9)^2}{23^2} < 1, \quad (4.1)$$

the population contained 14,914 stars with mean velocities $(\bar{U}, \bar{V}, \bar{W}) = (-10.0 \pm 0.2, -13.3 \pm 0.1, -6.8 \pm 0.1) \text{ km s}^{-1}$ and standard deviations $(U_{s.d.}, V_{s.d.}, W_{s.d.}) = (22.2, 13.2, 8.6)$ (figure 3). This ellipsoid contains the bulk of stars with conventional thin disc orbits. A substantial number, 5,660, of fast moving stars have been discarded. The remaining distributions are close to Gaussian (bearing in mind the expected asymmetry of the V distribution). The ellipsoid has axes $(3.2\sigma_U, 3.0\sigma_V, 2.7\sigma_W)$. The ratio between the standard deviations of this sample, 2.6:1.5:1, is close to that found by Dehnen and Binney (1998), 2.2:1.4:1.

Although the U -distribution is expected to be symmetric while the V -distribution is not, there is a greater discrepancy between \bar{U} and U_e than there is between \bar{V} and V_e . We will understand this as a consequence of streaming motions. In the absence of a full understanding of the dynamics underlying streams, it is strictly not possible to give an estimate of U_0 from either \bar{U} or U_e . We have adopted an estimate from \bar{U} , in keeping with usual practice, but without detailed understanding of the causes of asymmetry in the U distribution, one should be cautious of placing much reliance on it.

5 Parenago's Discontinuity

We restricted the population to 8,098 dwarfs and binned by colour into 20 bins, each with close 400 members. We plotted $-\bar{U}, -\bar{V}, -\bar{W}$ and

$$\sigma_R = \sqrt{v_R^2}$$

against $B - V$ for the bins, where v_R is radial velocity from Sgr A* (figure 4). Parenago's discontinuity is seen in the plots of σ_R (purple) and $-\bar{V}$ (red): around $B - V = 0.64 \text{ mag}$ (type G3-4), there is an abrupt change in gradient from a strongly positive value to about zero. Dehnen & Binney suggest that the reason for Parenago's discontinuity is the heating of the disc, scattering processes

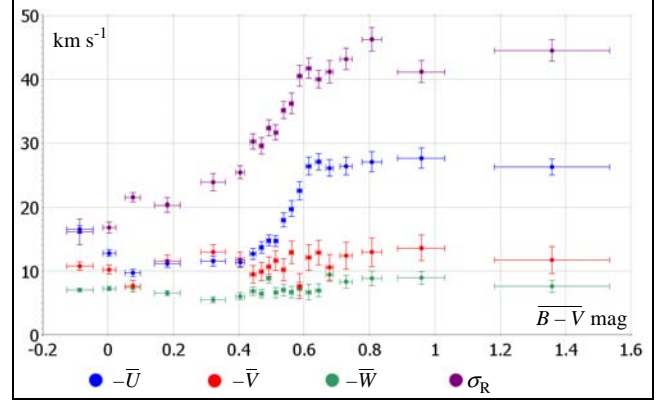


Figure 4: Solar motion, $(-\bar{U}, -\bar{V}, -\bar{W})$ and σ_R , relative to stellar populations binned by colour. The horizontal axis shows $B - V$ for each bin with standard error bars.

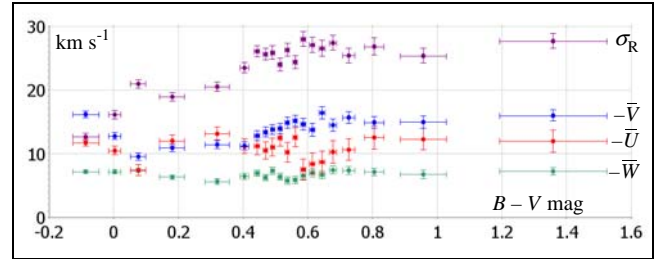


Figure 5: As figure 4, for stars within the velocity ellipsoid.

causing the random velocities of stars to increase with age (e.g., Jenkins 1992). Bluer stars to the left of the discontinuity reflect younger populations, while those to the right of the discontinuity have an age equal to that of the Galactic disc. On the face of it, this would suggest an age of about 10 Gyrs for the Galaxy.

We restricted the population to the velocity ellipsoid (figure 5). The sharp rise above $B - V = 0.4 \text{ mag}$. was eliminated, showing that Parenago's discontinuity is caused by fast moving stars rather than by gradual heating. Quillen & Garnett (2000) found an abrupt, statistically significant, jump in all velocity components at age $9 \pm 1 \text{ Gyrs}$, corresponding roughly to Parenago's discontinuity, and proposed that the cause might be a galactic merger. It will be only possible to interpret these results by analysing the age and composition of the various stellar streams (sections 7 & 8). We will find that these effects are associated with the Hercules stream.

Population	Region	Stars	\bar{U}	\bar{V}	\bar{W}	$U_{s.d.}$	$V_{s.d.}$	$W_{s.d.}$	V_0 (th.)
All stars	All	19,318	-10.2±0.2	-17.8±0.2	-7.4±0.1	32.5	21.2	15.8	8.2±0.6
All F&G dwarfs	All	8,124	-10.7±0.4	-18.1±0.2	-7.4±0.2	33.7	21.4	16.6	7.8±0.7
G-CS F&G dwarfs	All	6,691	-10.4±0.4	-18.1±0.3	-7.4±0.2	33.2	21.2	16.6	8.1±0.7
All K&M giants	All	4,815	-8.9±0.5	-20.0±0.3	-7.5±0.3	34.3	22.3	17.4	9.3±0.8
Famaey K&M giants	All	3,295	-7.9±0.6	-20.4±0.4	-7.7±0.3	34.2	22.3	17.4	9.8±0.8
All stars	Ellip	14,914	-9.9±0.2	-13.2±0.1	-6.8±0.1	22.8	13.4	8.7	8.5±0.3
All F&G dwarfs	Ellip	5,630	-10.4±0.3	-13.8±0.2	-6.7±0.1	23.9	13.6	9.2	8.6±0.4
G-CS F&G dwarfs	Ellip	4,610	-10.4±0.4	-14.1±0.2	-6.7±0.1	24.3	13.9	9.4	8.7±0.4
All K&M giants	Ellip	3,071	-8.4±0.4	-14.3±0.3	-6.7±0.2	24.4	14.2	9.3	8.9±0.4
Famaey K&M giants	Ellip	2,077	-7.7±0.5	-14.7±0.3	-6.6±0.2	24.1	13.9	9.3	9.4±0.5

Table 3: Calculated mean velocities and standard deviations for different populations, together with the value of V_0 corrected for the asymmetric drift using the theoretical and empirical values of D . The restriction to G-CS and to Famaey shows little difference from the distributions for F&G dwarfs or K&M giants. Statistical errors are likely to be understated for the full population because of the non-Gaussian nature of the distribution. The true error in V_0 is dominated by streaming bias.

6 Strömberg's Asymmetric Drift Relation

Strömberg's asymmetric drift equation (e.g., Binney and Tremaine, 1987, 4-34) can be written

$$\bar{V} = V_0 + \frac{\overline{v_R^2}}{D} \quad (6.1)$$

where v_R is radial velocity from Sgr A*. Using the theoretical value, $D = 110 \pm 7 \text{ km s}^{-1}$ given by Binney and Tremaine, we obtained, for the population of 20,574 stars,

$$V_0 = 8.2 \pm 0.6,$$

and, for 14,914 stars in the velocity ellipsoid,

$$V_0 = 8.5 \pm 0.3.$$

The major part of the error is due to uncertainty in D , but the error for the entire population may be understated because the distribution is not Gaussian. The reduced error for stars in the velocity ellipsoid is due both to the reduction in uncertainty in \bar{V} and to a reduced value of $\overline{v_R^2}$. We repeated the calculation for G-CS and Famaey to compare the results of these kinematically unbiased populations with the full populations of F&G dwarfs and K&M giants (table 3). Comparison between the figures indicates that statistical errors outweigh possible selection bias.

Strömberg's asymmetric drift equation (6.1) predicts a linear relation between V_0 and $\overline{v_R^2}$. It is generally thought that, in principle, one can plot a line of best fit, and read V_0 from the intersect with the vertical axis. Figure 6 shows the regression for dwarfs binned by colour. The two bluest bins represent populations of young stars which may be expected a kinematic behaviour different from the background. When they are excluded the intercept is $V_0 = 4.1 \pm 1.5$. Restriction to the velocity ellipsoid reduces both $-\bar{V}$ and $\overline{v_R^2}$, and leads to a consistent result but the quality of the regression is poor. There is no correlation for the fourteen bins with $B - V > 0.427$ (F3-4), indicating that the correlation has been produced by a population of fast moving stars, not by progressive changes in a well-mixed distribution.

The method strictly requires a kinematically unbiased population. We repeated the exercise for G-CS and Famaey. We found no useful correlation for the giants. For G-CS the intercept was found at $V_0 = 3.8 \pm 1.5$. The two reddest bins in G-CS lie outside of the line of the rest of the population. When they are excluded the intercept drops to $V_0 = 1.1 \pm 1$. The results of these calculations show larger than expected errors. Examination of figures 1 and 3 suggests that they are unreasonable. $V_0 < 6$ would imply that over 70% of the population trail the LSR. By a rough estimate, for a well-mixed distribution, the radial distance of a typical orbit to pericentre would be about half that to apocentre, and velocity dispersion would therefore be greater than it is by an approximate factor of four.

7 Bulk Streaming Motions

The existence of stellar streams was first established from astronomical investigations dating as far back as 1869 (Eggen, 1958). They were thought to consist of previously clustered coeval stars that have been gradually dispersed by the dynamic processes of tidal forces, differential galactic rotation, and encounters with other stars. Increasingly comprehensive star catalogues published in the 1950's opened the way for more thorough analyses. Beginning in 1958, O.J. Eggen produced a series of seminal studies of stellar streams using RA:DE proper motion ratios in conjunction with radial velocities. The results of Eggen's investigations realized significantly increased membership counts and spatial extents of stellar streams. Eggen hypothesized a more protracted process of dissolution for star clusters. In Eggen's scenario, as star clusters dis-

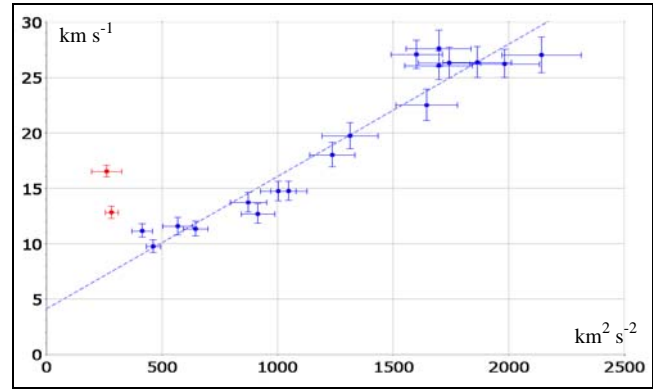


Figure 6: $-\bar{V}$ against $\sigma_R^2 = \overline{v_R^2}$ binned by colour. The line of regression is shown, excluding $B - V < 0.057$.

solve during their journeys around the Galaxy, they are stretched into tube-like formations which were subsequently called superclusters.

The investigation of stellar streams received a major boost with the arrival of the precision astrometry afforded by the Hipparcos mission. Dehnen (1998), using transverse velocities derived from Hipparcos, produced accurate maps of the local stellar velocity distribution showing that streams contain a significant proportion of late type stars. A wide range of stellar ages was identified within superclusters, challenging Eggen's hypothesis of common origin (e.g., Chereul et al., 1998, 1999). Building on the theoretical groundwork of Kalnajs (1991), Dehnen (1998) described a mechanism in which the outer Lindblad resonance of the Galactic bar could elongate closed orbits (in two modes) near the solar circle. Dehnen (1999, 2000) called its predicted effect "resonant scattering" and identified a clear signature in the Hipparcos data. This mechanism appears to work well for the Hercules stream (Fux, 2001).

Streams are not necessarily all formed in the same way and the search for other types of dynamical mechanisms to account for the Sirius, Hyades and Pleiades streams is ongoing. Candidates include migrations of resonant islands (Sridhar & Touma, 1996; Dehnen, 1998) and transient spiral waves (De Simone et al., 2004; Famaey et al., 2005) in which streams originate from perturbations in the gravitational potential associated with spiral structure.

Famaey et al. (2005) described six kinematic groups: three streams, Hyades/Pleiades, Sirius and Hercules, a group of young giants, high velocity stars and a smooth background distribution (figure 11). We smoothed the velocity distribution by replacing each discrete point with a two dimensional Gaussian function and finding the sum. A standard deviation of 0.5 gave a clear contour plot (figure 12). We distinguish the Hyades and Pleiades streams, since the velocity distributions shows separate peaks, and, as we will see, these streams contain different distributions of stellar types and ages. There is a large and well dispersed stream centred at $(U, V) = (25, -23)$, noted by Dehnen (1998). We have called it the Alpha Ceti stream, after the brightest star we identified with stream motions (this is not a guarantee of stream membership, but makes it probable).

Figures 13 - 17 show changes in the velocity distribution with respect to stellar type. More detailed information about the structure of streams was also gleaned using narrower colour bands. There are few candidates for the Sirius and Hyades streams earlier than B7, and these appear to be part of the distribution for stars with

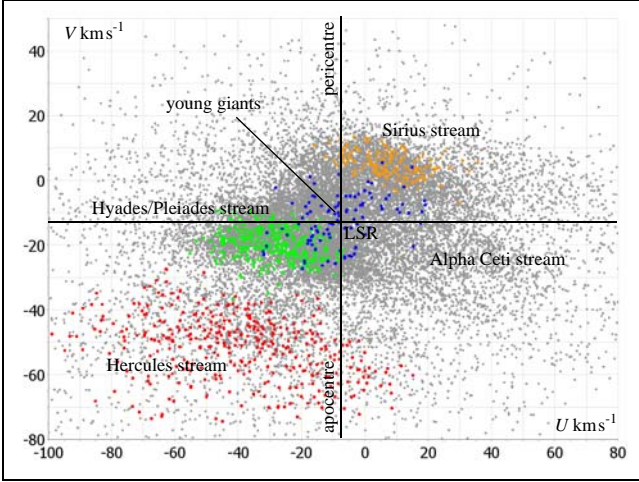


Figure 11: U - V plot showing groups identified by Famaey et al. (2005). These represent only a small proportion of the true membership of the streams. The calculated position of the LSR is shown for clarity only.

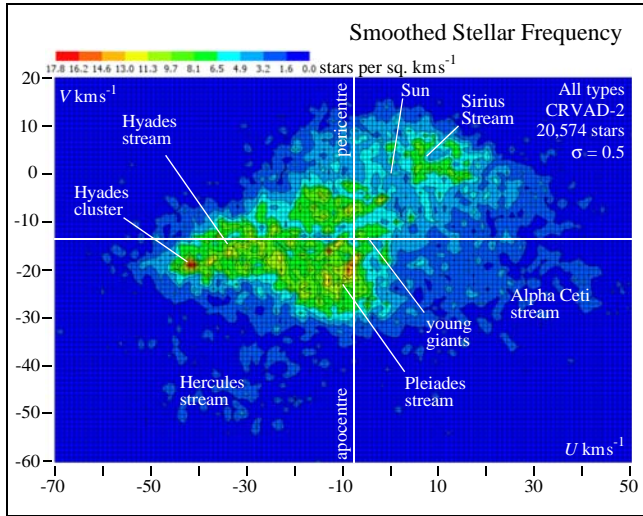
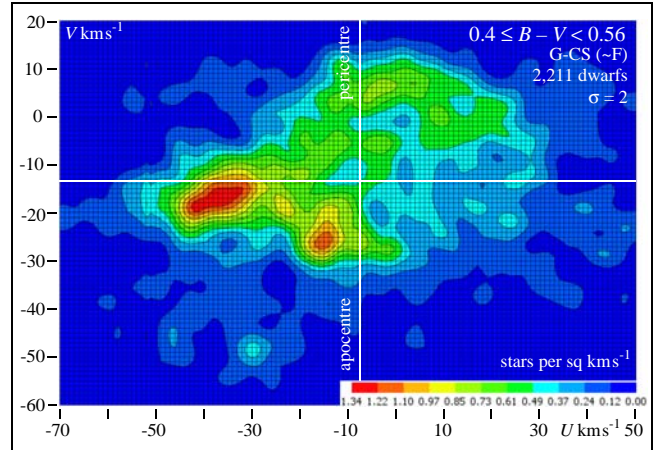
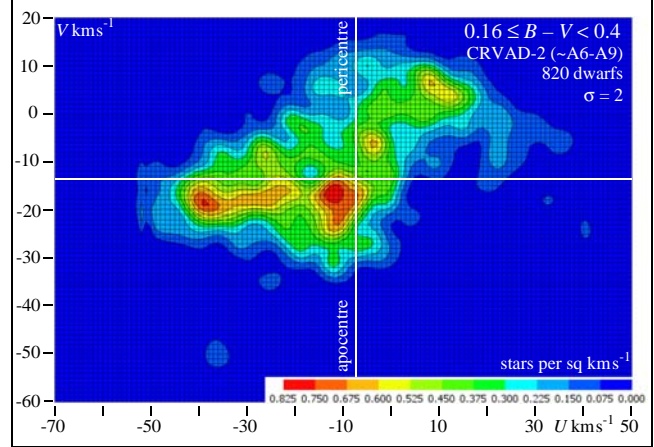
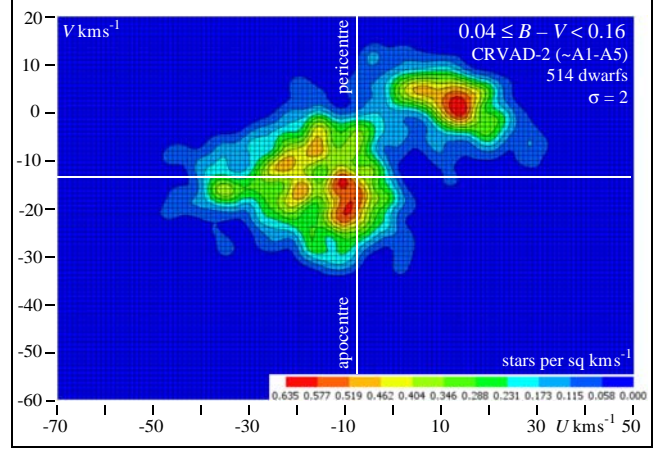
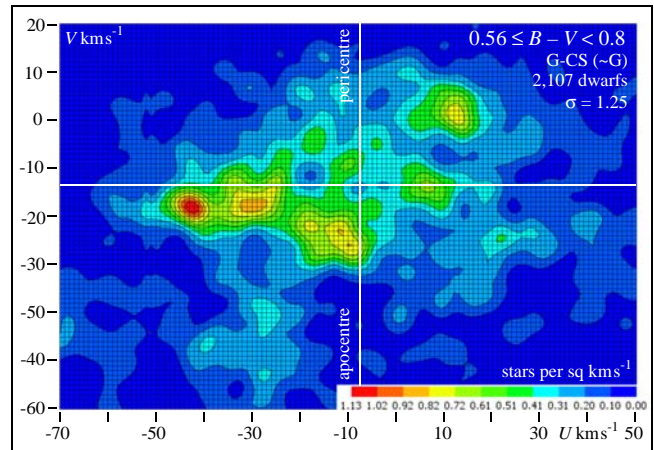
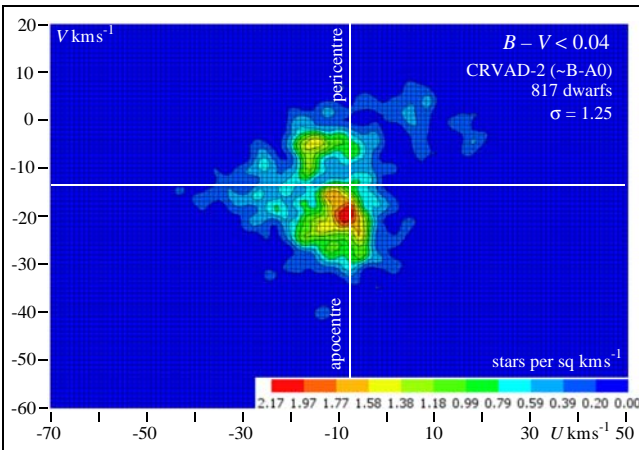


Figure 12: The distribution of U - and V -velocities using Gaussian smoothing with a standard deviation of 0.5 km s^{-1} , showing the Hyades, Pleiades, Sirius, Alpha Ceti and Hercules streams.

Figures 13 - 17: The variation of the velocity distribution with respect to stellar type. Density contours are relative to the peak density for each plot. The optimal choice of σ is subjective and depends on stellar density. Too high a value will suppress details of structure, while too low a value may cause random fluctuations to appear as structure.



young kinematics. The earliest indication of the Sirius stream as a distinct distribution is for stars of type B8, corresponding to an age of about 300 Myrs, and for the Hyades stream for type B9, an age of about 400 Myrs. The Hercules and Alpha Ceti streams are both apparent at type F0, corresponding to an age of about 2½ Gyrs, with too few candidates of earlier types to draw conclusions.

Comparison of the distributions in figures 13 - 17 with figure 4 shows that the values of $-\bar{V}$ and σ_R for different types depends heavily on the structure of the velocity distribution. The bluest stars reflect recent star formation in the Pleiades stream, leading to a low value of σ_R . For $0.04 \leq B - V < 0.16$, the velocity distribution is concentrated in the Pleiades and Sirius streams, resulting in a rise in σ_R and the minimum of $-\bar{V}$ seen in figure 4. For $0.16 \leq B - V < 0.4$ the Hyades stream begins to dominate, resulting in the increased values of both $-\bar{V}$ and σ_R . Finally, for F & G dwarfs, the Hercules and Alpha Ceti streams cause further increases in $-\bar{V}$ and σ_R , seen leading up to Parenago's discontinuity in figure 4, and the reduced importance of the Sirius stream also causes $-\bar{V}$ to increase.

In conclusion, dependencies on colour show that stream membership is underestimated in Famaey's figures. The increasing value of $-\bar{V}$ with respect to colour is seen in the figures 12 - 17, and depends heavily on stream composition. The slope of the regression in figure 6 is dictated by the structure of the velocity distribution, and has little or no bearing on Strömberg's asymmetric drift equation. Streams violate the assumption of a well-mixed distribution; we cannot determine the value of D empirically through binning the population by type or by colour.

Gas clouds from which stars form are expected to have a more nearly circular motion than the norm. Recently formed stars can be expected to have a more nearly circular motion than the population as a whole. The Pleiades stream is seen in figures 11 to 13 to have a strong peak in the vicinity of $(U, V) = -10 \pm 2, -16 \pm 3$. Although this does not give a precise estimate of the LSR, it may be regarded as a rough guide to the vicinity of velocity space in which the LSR is to be found.

8 Old Stars

It might be expected that a population of old stars will be sufficiently well-mixed to carry out a calculation of the asymmetric drift. G-CS II isochrone ages appear to be at least broadly reasonable, and were supported by an H-R diagram showing age bands in accordance with theory, to be reported in a paper in preparation. An explanation for the number of old stars in the Hyades cluster has been found and will also be reported. There are known problems with isochrone aging for very young stars; we found that a substantial number of stars with young kinematics had been assigned ages greater than 13 Gyrs. We binned G-CS into age groups of 1Gyr and calculated $-\bar{U}$, $-\bar{V}$, $-\bar{W}$ and V_0 for each population using $D = 90 \pm 20$, which gives a measure of agreement for the younger populations with our previous values (figure 18). $-\bar{V}$ rises dramatically with age and there is a sudden shift in the calculated value of V_0 at 9 Gyrs. However, plots of the velocity distribution show that a well-mixed population has not been found (figures 19 & 20). The changes in $-\bar{V}$ and V_0 are caused by the reduced importance of the Sirius stream and the increased prominence of the Hercules and Alpha Ceti streams in the bins of age greater than 9 Gyrs. It is possible to identify that these are streams of older stars and that the rise in $-\bar{V}$ and σ_R with $B - V$ in figure 4 is due to the influence of these streams, not gradual heating.

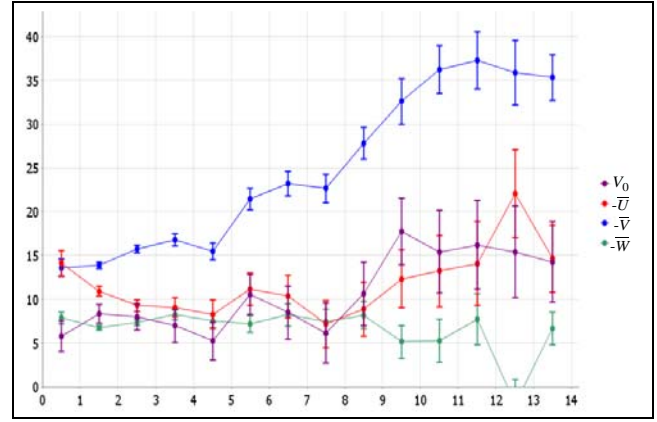


Figure 18: Values of $-\bar{U}$, $-\bar{V}$, $-\bar{W}$ and V_0 for populations in 1Gyr bins, using $D = 110 \pm 20$. The midpoint of the bin is shown. Connecting lines are drawn for clarity. The last bin contains all stars given as > 13 Gyrs, and is likely to contain a number of very young stars.

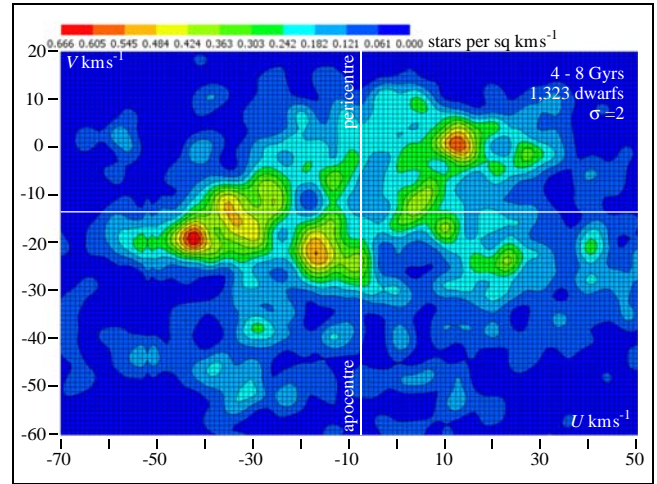


Figure 19: The U - V density for stars aged between 4 and 8 Gyrs. Nine members of the Hyades cluster are contained in this group.

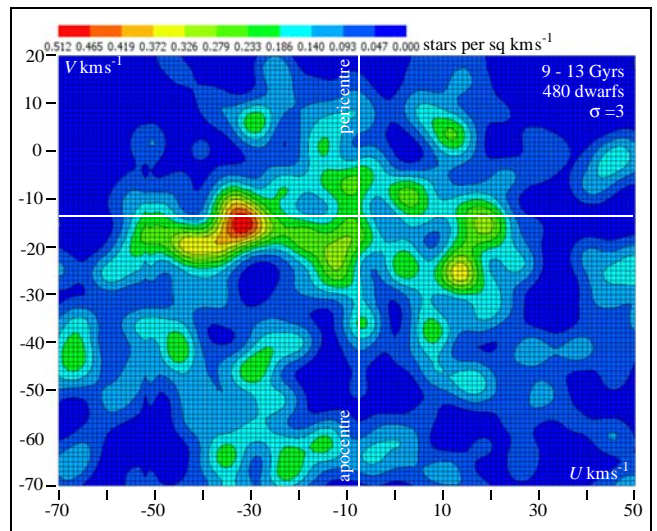


Figure 20: The U - V density for stars aged between 9 and 13 Gyrs. Four members of the Hyades cluster are contained in this group.

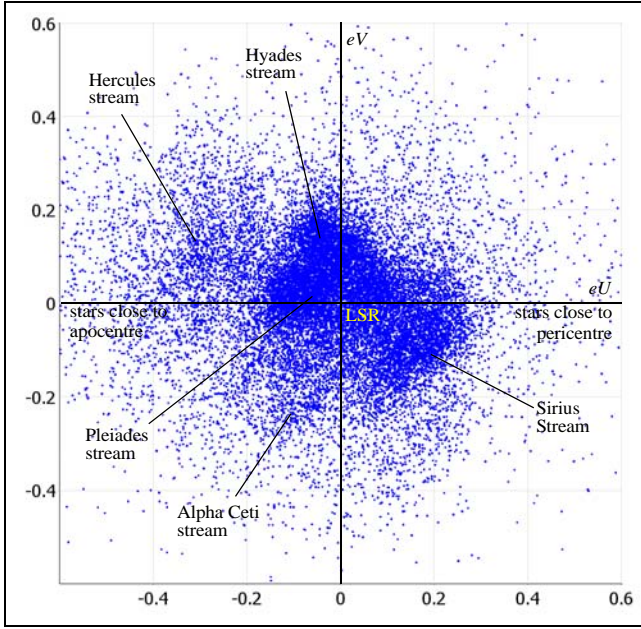


Figure 21: The distribution of eccentricity vectors is not homogeneous in the U - V plane. The plot is based on our best estimate of the LSR.

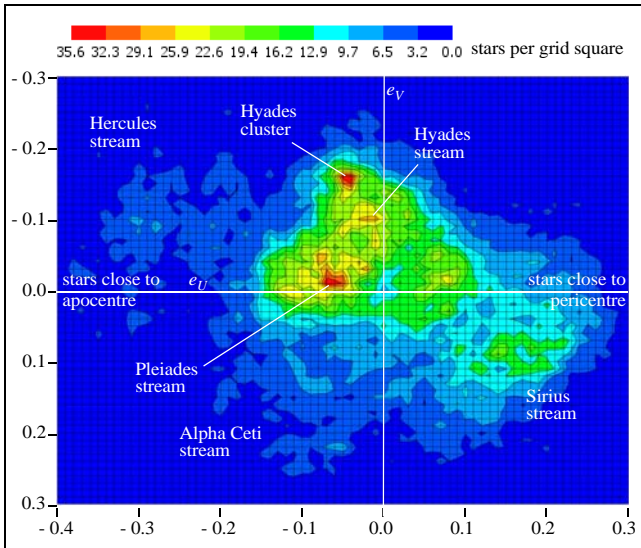


Figure 22: Contour of the density of the eccentricity distribution. The Hercules stream has eccentricities up to ~ 0.3 and orbits approaching apocentre. The Sirius and Alpha Ceti streams have eccentricities ~ 0.1 - 0.25 approaching pericentre. The Hyades stream has eccentricities below ~ 0.2 approaching apocentre. The Pleiades stream has eccentricities below ~ 0.1 close to apocentre.

9 The Eccentricity Distribution

For an elliptical orbit the eccentricity vector is defined as the vector pointing toward pericentre and with magnitude equal to the orbit's scalar eccentricity. It is given by

$$\mathbf{e} = \frac{|\mathbf{v}|^2 \mathbf{r}}{\mu} - \frac{(\mathbf{r} \cdot \mathbf{v}) \mathbf{v}}{\mu} - \frac{\mathbf{r}}{|\mathbf{r}|} \quad (9.1)$$

where \mathbf{v} is the velocity vector, \mathbf{r} and $\mu = GM$ is the standard gravitational parameter for orbits about a mass, M . For a Keplerian orbit the eccentricity vector is a constant of the motion. Stellar orbits are not strictly elliptical because mass is distributed in the disc and in the halo. In addition, the orbit will oscillate in the W -direction due

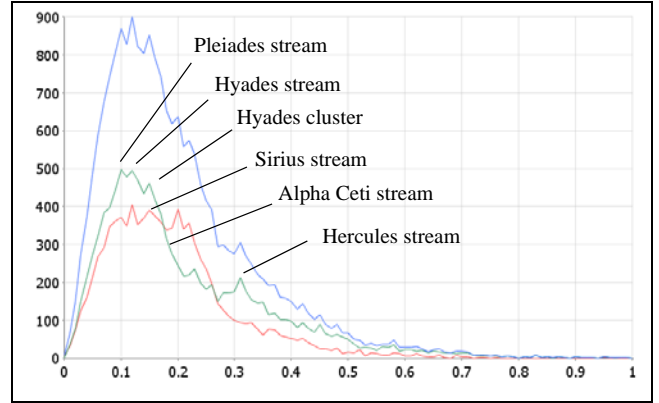


Figure 23: Eccentricity distribution (based on the LSR found in this paper) for the entire population (red), for stars closer to apocentre (blue) and stars closer to pericentre (green), as defined by position with respect to the semi-latus rectum. The number of stars closer to apocentre is expected to outweigh the number closer to pericentre, by at most about 20% for $e = 0.1$, and more for larger eccentricities

to the gravitational attraction of the disc, rather than being truly planar. The eccentricity vector is expected to precess from both these causes, generating a rosette. Nonetheless, the orbit will approximate an ellipse at each part of its motion, and the eccentricity vector remains a useful measure. Over time the eccentricity vectors of different stars will precess at different rates. It is usually assumed that, in time, an equilibrium state will be attained in which the distribution is well-mixed.

In a well-mixed population the eccentricity vectors will be spread smoothly in all directions, with an overdensity at apocentre and underdensity at pericentre, because of the increased orbital velocity at pericentre and because stars at apocentre come from a denser population nearer the galactic centre. This is not seen in a plot of the distribution of eccentricity vectors (figure 21). In practice stellar streams are found in which the eccentricity vectors are concentrated at particular values. We smoothed the eccentricity distribution by replacing each discrete point with a two dimensional Gaussian function and finding the sum. Standard deviation, σ , is used as a smoothing parameter. A standard deviation of 0.005 gave a clear contour plot (figure 22) showing that mixing is poor. The structure of the distribution is largely determined from streaming motions.

10 Analysis with an Eccentricity Cut

A better representation of the velocity distribution of the thin disc may be found by discarding the velocity ellipsoid and instead restricting by eccentricity in the U - V plane, and restricting W -velocity to within a range centred on W_0 . For any given value of the LSR, and any e_0 with, $0 < e_0 < 1$, one may find a population of stars with eccentricity in the galactic plane less than e_0 . We found the best match between this population and Gaussian distributions. The advantages of this method are: a) it finds an estimate of the LSR directly, without a separate correction for asymmetric drift; b) cutting on eccentricity better represents the kinematic properties of stars in the thin disc; c) it uses fewer fitting parameters, so is less prone to statistical fluctuations; d) although streams are clearly apparent in the eccentricity distributions for stars closer to apocentre and stars closer to pericentre, as defined by position with respect to the semi-latus rectum (figure 23), the smooth form of the full distribution gives reason to hope that the effect of streaming motions

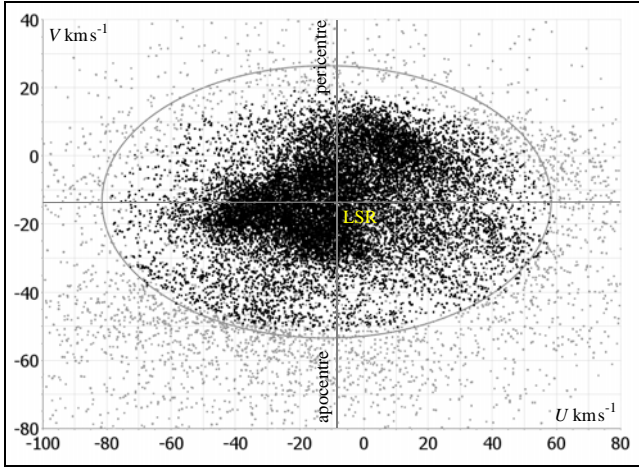


Figure 25: U - V , V - W , and U - W velocity plots for thin disc stars with eccentricities less than 0.32 and $|W + 6.8| < 22$ (black), compared to the velocity ellipsoid, shown in outline and the remaining population (grey).

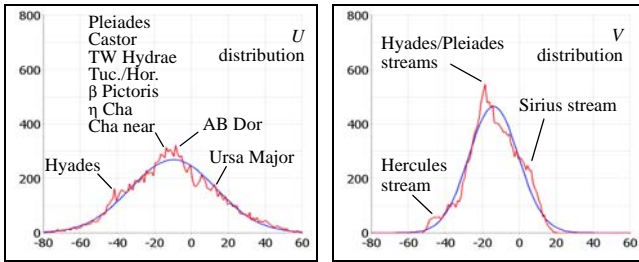


Figure 24: Velocity distributions for 15,634 stars with $|W + 6.8| < 23$ and eccentricity less than 0.32 compared to Gaussians with the same standard deviation. Positions of moving groups from Zuckerman & Song (2004).

balance in large degree. If this is the case, the LSR found by optimizing the fit will be close to the true value.

Four variables were used in the fit. We minimized the combined sum of U and V squared differences to find V_0 and the eccentricity bound, e_0 . U_0 was set to the mean of the previous iteration, and was found to converge. We also minimized W squared differences to find the bound on W -velocity and W_0 , which converged to a value close to the mean. The resulting population contained 15,634 stars with eccentricities less than 0.32 and with $|W + 6.8| < 23$ and gives an estimate of the LSR:

$$(U_0, V_0, W_0) = (-9.8 \pm 0.2, -13.2 \pm 1.3, -6.8 \pm 0.1) \text{ km s}^{-1}.$$

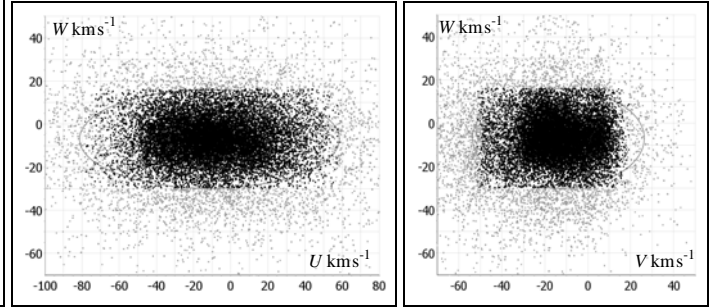
The velocity ellipsoid is now replaced with an elliptical cylinder. The statistical error in \bar{V} is less than that in V_0 :

$$\bar{V} = -13.9 \pm 0.4 \text{ km s}^{-1}.$$

The standard deviation is

$$(U_{s.d.}, V_{s.d.}, W_{s.d.}) = (23.2, 13.5, 9.5) \text{ km s}^{-1}.$$

Despite containing substantially more stars, the cylinder is more compact than the ellipsoid. For the observed local velocity distribution, the centre of the velocity ellipsoid is unexpectedly close to the LSR, but the asymmetric drift is seen in figure 25. The centre of the oval in the U - V plane is offset by about 5 km s^{-1} in the V -direction from the estimate of the LSR. This shows the effect of streaming bias; if the population were well-mixed, the centre of the velocity ellipsoid would be offset by a similar amount.



11 Circular Orbits

Over time, scattering events cause the random velocities of stars to increase with age (e.g., Jenkins, 1992), often described as heating of the disc. Even in thermal equilibrium, one would expect a modal value of random peculiar velocity denoting disc temperature. Circular motion represents an absolute zero temperature and can therefore be expected to be rare for mature orbits. It follows that a minimum in the velocity distribution can be expected at the LSR. In practice the situation is not so simple. Figure 12 shows a deep trough in the vicinity of $V = -12$, containing a number of minima. These do not give a precise estimate of the LSR.

We plotted the number of stars with eccentricity less than 0.01 for a range of values of U_0 and V_0 (figure 27). Eliminating the youngest population of blue stars causes the minima to both get both deeper and wider, in keeping with the notion that they are caused by a heating effect. $B - V < 0.3$ gave deep minima, but for $B - V < 0.4$ the minima become broader, and their positions less precise. The strongest candidate for the minimum at the LSR found at $(U, V) = (7.5 \pm 1.0, 13.5 \pm 0.3) \text{ km s}^{-1}$. We believe this is the best available estimate. Other candidates were finally rejected after analysis of the circular speed curve (section 12).

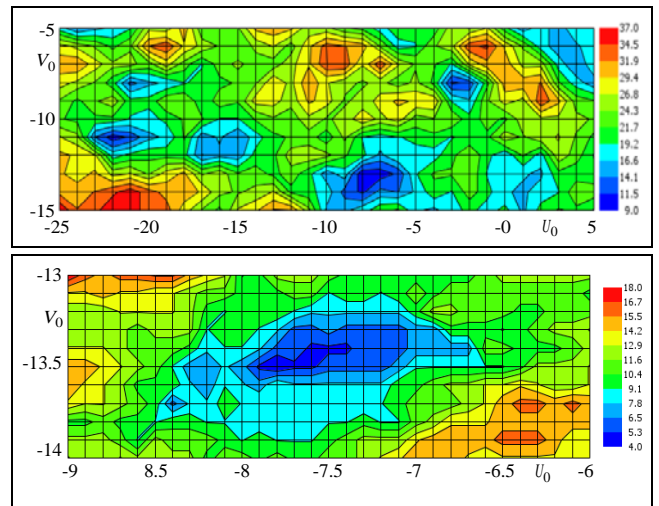


Figure 27: The number of stars with eccentricity less than 0.01 for different values of (U_0, V_0) , in multiples of 1 km s^{-1} , and focussing on the least minimum in multiples of 0.1 km s^{-1} . Stars with $B - V < 0.3$ are excluded. The position of the minimum gives our best estimate for the LSR, $(U_0, V_0) = (7.5 \pm 0.5, 13.5 \pm 0.3) \text{ km s}^{-1}$.

12 The Circular Speed Curve

We restricted the population to stars close to orbital extrema, having $|U - U_0| < 7 \text{ km s}^{-1}$, for a range of values of U_0 . We plotted the transverse orbital velocity against distance to SgrA*, based on an adopted transverse solar velocity of 225 km s^{-1} , and on the assumption that SgrA* is stationary at the Galactic barycentre. On this assumption, the proper motion of SgrA* determined by Reid and Brunthaller (2004) implies a distance to the Galactic centre of $7.44 \pm 0.04 \text{ kpc}$, consistent with recent determinations of the distance to SgrA* (Reid, 1993; Nishiyama et al., 2006; Bica et al., 2006; Eisenhauer et al., 2005; Layden et al., 1996). For values of $U_0 = 7.5 \pm 2.5$, the scatter plot of the distribution (figure 28) divides clearly into two parts, with a less densely populated band of stars which we believe to be on near circular orbits.

Young stars have velocities dependent on the kinematics of the gas clouds from which they are formed, and are suspected to have motions close to the LSR. We removed stars with $B - V < 0.3$. This increased the visual clarity of the split. There is a noticeable degradation in the quality of the split outside the range $U_0 = 7.5 \pm 0.5$. Outside of $U_0 = 7.5 \pm 2.5$ the split was barely visible (at this dot size). We believe that this confirms the figure $U_0 = 7.5 \pm 1$ found by calculating circular orbits (section 11) and eliminates the alternate minima.

We restricted distances to 160pc (because of the low population outside this range) and used Gaussian smoothing to find the density of the frequency distribution (figure 29). The trough was well displayed for a range of smoothing parameters, $0.3 \leq \sigma_v \leq 0.6$, $3 \leq \sigma_R \leq 6$. Too large values of the smoothing parameters cause interference between peaks in the difference and the minima, while too small values broke up the distribution excessively. We used regression to find a line of best fit to the minima at given distance from SgrA*. and found the intercept at 211.5 ± 0.5 , corresponding to $V_0 = 13.5 \pm 0.5$, and a slope of $-9.3 \pm 0.9 \text{ km s}^{-1} \text{ kpc}^{-1}$.

There is some uncertainty in the slope on account of the short distance for which the population is sufficiently dense to find a meaningful minimum in the trough. Moving groups with close to circular motion also increase uncertainty. However, the existence of the trough in the distribution is significant. The method for calculating both the LSR and the circular speed curve will become more valuable when data from Gaia becomes available. It will be potentially be possible to extend the analysis to a much larger region of space, perhaps even to trace the rotation curve to near the centre of the Galaxy, and a similar distance outward from the Sun where current methods are problematic.

13 Conclusions

The velocity distribution of local stars is highly structured, and heavily biased towards membership of five major streams. The distribution of stream membership contains dependencies on both colour and age. These dependencies, not Strömberg's asymmetric drift relation, are responsible for the correlations between \bar{V} and σ_R^2 from which the asymmetric drift is usually calculated, and invalidate the usual calculation of the LSR, for which a well-mixed distribution is required.

Given the highly structured velocity distribution of the local population, standard statistical measures may be of little use in ascertaining the local standard of rest. We found alternative indicators by examining the properties of the velocity distributions. We believe the best indicators are based on an observed (and unanticipated) minimum in the distribution which we believe represents circular motion. We have accounted for this minimum as a conse-

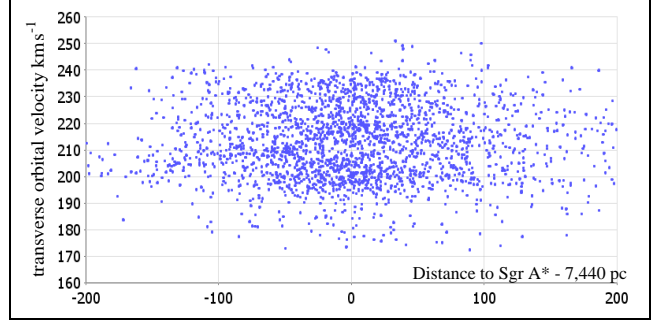


Figure 28: Transverse orbital velocities of 2,350 stars with $|U + 7.5| < 7$ plotted against distance to SgrA*. The slope of the circular speed curve is seen in the dearth of stars on circular orbits.

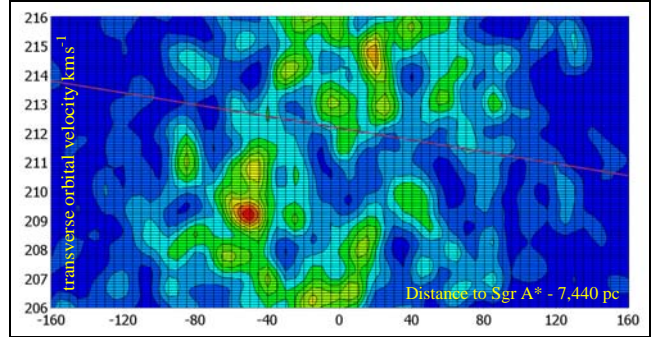


Figure 29: The transverse velocity distribution of stars close to circular motion within $206 < V_T < 216$, excluding stars with $B - V < 0.3$, using Gaussian smoothing with parameters $\sigma_v = 0.4$ $\sigma_R = 5$. The line of regression through the minima at constant distance is also shown. The correlation is significant at 99%

quence of heating of the disc. A more rigorous argument will require detailed analysis of the relationship between streams and spiral structure, which is the subject of a paper in preparation. The analysis will support the notion that the minimum represents circular motion. An important strength of the method is that it is unaffected by the dynamical properties of moving groups and streams with non-circular motions.

We found a good measure of agreement between methods (table 4). Our best estimate of the LSR is $(U_0, V_0, W_0) = (7.5 \pm 1.0, 13.5 \pm 0.3, 6.8 \pm 0.1) \text{ km s}^{-1}$. W_0 is found from the mean after restricting the population by Gaussian fitting. U_0 and V_0 are found from the low frequency of stars in orbits with eccentricity less than 0.01, supported by the observed trough in the distribution for stars close to orbital extrema, from which we have derived the slope of the circular speed curve on the assumption that the trough corresponds to circular motion. These figures are consistent with the supposition that SgrA* is stationary at the Galactic barycentre at a distance of $7.4 \pm 0.2 \text{ kpc}$ and a Solar transverse orbital velocity of $225 \pm 9 \text{ km s}^{-1}$.

We calculated the local slope of the circular speed curve found from the low frequency of circular orbits. An unbiased estimate was found by restricting the population to stars close to orbital extrema. For 2,350 stars with $|U + 7.5| < 7 \text{ km s}^{-1}$ and $B - V > 0.3$ the correlation is significant at 99%, and the slope is $-9.3 \pm 0.9 \text{ km s}^{-1} \text{ kpc}^{-1}$. A slope of this magnitude suggests that the local mass distribution does not reflect a smooth global distribution of dark matter. Data from Gaia will make it possible to use this low density to trace the rotation curve over much greater distances.

Table 4: Peculiar Solar Motion
Summary of Results

Method	U_0 kms ⁻¹
Mean, all stars	10.2 ± 0.2
Mean, velocity ellipsoid	10.0 ± 0.2
Mean, eccentricity cut	9.8 ± 0.2
Young stars	-10 ± 2
Circular orbits	7.5 ± 1.0
Circular speed curve	7.5 ± 1.0

Method	V_0 kms ⁻¹
Young stars	-16 ± 3
Eccentricity cut	13.2 ± 1.3
Circular orbits	13.5 ± 0.3
Circular speed curve	13.5 ± 0.5

Method	W_0 kms ⁻¹
Velocity ellipsoid	6.8 ± 0.1
Eccentricity cut	6.8 ± 0.1

Because of the differences in methodology and possible systematic errors, it is not possible to use these figures for a best combined estimate. Our preferred estimates are **bolded**. The velocity ellipsoid and eccentricity cut methods are both subject to systematic bias due to streaming motions.

References

- Barbier-Brossat M., Figon P., 2000, A&AS, 142, 217B
 Bica E., Bonatto C., Barbuy B., Ortolani S., 2006, A&A, 450, 1, pp.105-115.
 Binney J.J., Dehnen W., Houk N., Murray C.A., Penston M.J., 1997, ESA SP-402, Hipparcos-Venice'97, p. 473
 Binney J.J., Tremaine S., 1987, Galactic Dynamics, Princeton Univ. Press, Princeton
 Bobylev V. V. Gontcharov G. A. Bajkova A. T., 2006, Astronomy Reports, 50, 9, 733-747.
 Bobylev V. V. & Bajkova A. T., 2007, 3D Space Astronomicheskii Zhurnal, 2007, Vol. 84, No. 5, pp. 418-428.
 Chereul E., Cr ez e M., Bienaym e O., 1998, A&A, 340, 384
 Chereul E., Cr ez e M., Bienaym e O., 1999, A&A, S135, 5
 Dehnen W., 1998, Ap. J., 115, 2384
 Dehnen W., 1999, Ap. J. 524, L35-L38
 Dehnen W., 2000, Ap. J. 119, 800
 Dehnen W. & Binney J.J. 1998, MNRAS 298, 387.
 Eggen O.J., 1958, MNRAS, 118, 65
 ESA, 1997, The Hipparcos and Tycho Catalogues, ESA SP-1200
 Eisenhauer F., Genzel R., Alexander T., Abuter R., Paumard T., Ott T., Gilbert A., Gillessen S., Horrobin M., Trippe S., Bonnet H., Dumas C., Hubin N., Kaufer A., Kissler-Patig M., Monnet G., Str obele S., Szeifert T., Eckart A., Sch odel R., & Zucker S., 2005, Astrophys. J., 628, 246-259
 Famaey B., Jorissen A., Luri X., Mayor M., Udry S., Dejonghe H., Turon C., 2005, Local Kinematics of K and M Giants from CORAVEL/Hipparcos/Tycho-2 Data, Astron. Astrophys. 430, 165
 Fehrenbach Ch., Duflo M., Burnage R., 2001, A & A 369, 65-73
 Fux R., ASP Conference Series, Vol. 228. Edited by S. Deiters, B. Fuchs, R. Spurzem, A. Just, and R. Wielen. San Francisco: Astronomical Society of the Pacific. ISBN: 1-58381-060-9, 2001., p.283
 Gray R. O., Corbally C. J., Garrison R. F., McFadden M. T., Bubar E. J., McGahee C. E., O'Donoghue A. A., Knox E. R., 2006, Contributions to the Nearby Stars (NStars) Project: Spectroscopy of

- Stars Earlier than M0 within 40 pc-The Southern Sample, Astrophys J., 132, 161G
 Gray R. O., Corbally C. J., Garrison R. F., McFadden M. T., Robinson P. E., 2003, Contributions to the Nearby Stars (NStars) Project: Spectroscopy of Stars Earlier than M0 within 40 Parsecs: The Northern Sample, Astrophys J., 126, 2048G.
 Hogg D. W., Blanton M. R., Roweis S. T., Johnston K. V., 2005, Astrophys.J., 629, 268-275.
 Houk N., Cowley A. P., 1975; Michigan Catalogue of HD stars, Vol. 1 VizieR On-line Data Catalog: III/31B
 Houk N., 1978, Michigan Catalogue of HD stars, Vol. 2, VizieR On-line Data Catalog: III/51B
 Houk N., 1982, Michigan Catalogue of HD stars, Vol. 3, VizieR On-line Data Catalog: III/80
 Houk N., 1988, Michigan Catalogue of HD stars, Vol. 4, VizieR On-line Data Catalog: III/133
 Houk N., 1999, Michigan Catalogue of HD stars, Vol. 5, VizieR On-line Data Catalog: III/214
 Jaschek C., & Valbousquet A. 1991a, A&A, 242, 77
 Jaschek C., & Valbousquet A. 1992b, A&A, 255, 124
 Jaschek M., 1978, Selected MK Spectral Types, Bull. Inform. CDS 15, 121; VizieR On-line Data Catalog: III/42
 Jenkins A., 1992, MNRAS, 257, 620
 Kalnajs A.J., 1991, in Sundelius B., ed., Dynamics of Disc Galaxies, G teborg, Sweden, p. 323
 Kharchenko N. V., Scholz R.-D., Piskunov A. E., R oser S., Schilbach E., Astron. Nachr., 328, 9, 889 (arXiv:0705.0878)
 Klypin A, Zhao H., and Somerville R. S., 2002, Ap. J., 573, 597-613
 Holmberg J., Nordstr om B. Andersen J., 2007, A&A, 475, 519-537.
 Layden A. C., Hanson R. B., Hawley S. L., Klemola A. R., & Hanley C. J. 1996, AJ, 112, 2110.
 van Leeuwen F., 2007a, Hipparcos, the New Reduction of the Raw Data, Springer
 van Leeuwen F., 2007b, Validation of the New Hipparcos Reduction, Astron.Astrophys. 474, 653V
 Mayor, 1974, A&A, 32, 321
 Mignard J., 2000, A&A 354, 522-536.
 Mihalas & Binney (1981) Galactic astronomy: Structure and kinematics, 2nd ed.
 Miyamoto M., and Zhu Z., 1998, AJ, 115, 1483.
 Nishiyama S., Nagata T., Sato S., Kato D., Nagayama T., Kusakabe N., Matsunaga N., Naoi T., Sugitani K., and Tamura M., 2006, Ap. J. 647, pt 1 pp. 1093-1098.
 Nordstr om B., Mayor M., Andersen J., Holmberg J., Pont F., J rgensen B.R., Olsen E.H., Udry S., Mowlavi N., 2004, The Geneva-Copenhagen survey of the Solar neighbourhood, A.&A., 419, 989.
 Quillen A.C. & Garnett D.R., 2000, <http://arxiv.org/abs/astro-ph/0004210v3>
 Reid M. J., 1993, ARA&A, 31, 345.
 Reid M. J. & Brunthaller A., 2004, Astrophys J., 616, 872-884.
 de Simone R.S., Wu X., & Tremaine S., 2004, MNRAS, 350, 627D
 Skuljan J., Hearnshaw J. B., Cottrell P. L., 1999, MNRAS, 308, 731-740
 Skiff B.A., 2007, Catalogue of Stellar Spectral Classifications, VizieR On-line Data Catalog: B/mk
 Str omgren, B. 1987, In 'The Galaxy', eds. Gilmore, G., and Carswell, R., (Dordrecht: Reidel), p. 229.
 Sridhar S. & Touma J., 1996, MNRAS, 279, 1263.
 Wright, C. O., Egan, M. P., Kraemer, K. E., Price, S. D., 2003, The Tycho-2 Spectral Type Catalog, Astrophys J., 125, 359W.
 Zuckerman B. & Song I., 2004, Annu. Rev. Astro. Astrophys. 42, 685-721.